Fast failure prediction of adhesively bonded structures using a coupled stress-energetic failure criterion

Jérémy Le Pavic, Georgios Stamoulis, Thomas Bonnemains, David da Silva, David Thevenet

Fast failure prediction of adhesively bonded structures using a coupled stress-energetic failure criterion

Jérémy Le Pavic[1,3] | Georgios Stamoulis[2] | Thomas Bonnemains[2] | David Da Silva[3] | David Thévenet[1]

[1]UMR CNRS 6027, IRDL, Ensta Bretagne, Brest, France

[2]UMR CNRS 6027, IRDL, Univ. Bretagne Occidentale, Brest, France

[3]ArianeGroup, Rue du Général Niox, Saint Médard en Jalles, France

Correspondence
Jérémy Le Pavic, UMR CNRS 6027, IRDL, Ensta Bretagne, F-29200 Brest, France.
Email: jeremy.le_pavic@ensta-bretagne.org

Funding information
ArianeGroup

Abstract

The use of adhesively bonded joints in industrial structures requires reliable tools for the estimation of the failure load. The necessary and sufficient condition to predict the strength of such joints involves the implementation of a coupled stress and energetic criteria. However, its application necessitates the identification of the stress distribution along the adhesive layer, which has been approximated in this paper by a previously published closed-form solution. This analysis along with finite element modelling results are compared with experimental data issued from a double-notched sample tested with the Arcan fixture at various load ratios. The results show good agreement; the use of the closed-form solution permitted to predict the failure load more rapidly and in a conservative manner compared with the experimental results. The application of the methodology is also extended to a wider range of joint geometries by means of spatial interpolation using the Kriging model.

KEYWORDS

adhesive bonding, coupled criterion, failure load prediction, Kriging, semianalytical

a, crack length; a^*, internal length to solve the coupled criterion; A, matrix of the semivariogram; A_{inc}, dimensionless parameter for energetic criterion resolution; b, width of the Arcan substrate; B, semivariogram vector of the unknown point; E, Young modulus; E^{eq}, equivalent modulus for plane strain hypothesis; $F^{fail,}$, failure load of the bonded structure; G^c, critical energy released rate; G_I^C, critical energy released rate in mode I; G_{II}^C, critical energy released rate in mode II; G_{inc}, incremental energy released rate for FEA application; G_{SA}, incremental energy released rate for semianalytical application; h, distance between two points for Kriging estimation; h_1, height of the Arcan substrate; H_{Plate}, height of the plate for the application section 3; k_{struct}, dimensionless parameter for stress criterion resolution; L, length of the Arcan substrate; $\tilde{L}$, remaining bonded length for semianalytical application; L^c, characteristic length of the bonded structure; L_{notch}, notch length of the sample; L_{rc}, bondline length; $L_{Subin\ f}$, length the lower plate for the application section 3; $L1_{plate}$, length the plate 1 for the application section 3; $L2_{plate}$, length the plate 2 for the application section 3; m, number of known points; M_{ij}, moment for the sandwich model; N_{ij}, normal force for the sandwich model; ND, normal displacement; NF, normal force; p, height under the beak of the Arcan substrate; P_i, known points for Kriging estimation; P_u, unknown points for Kriging estimation; r^o, ratio of multiaxiality; S_c, maximum shear stress; S_p, standard error deviation; t, bondline thickness; t_{adh}, bondline thickness for the application section 3; t_{ext}, thickness of the adherent for the application section 3; T_{ij}, tangential force for the sandwich model; TD, tangential displacement; TF, tangential force; W, weighting vector of the unknown point; W_i, weighting of the known points; W^T, transpose vector $\mathbf{W}$; Z_N, maximum normal stress; ε, strain applied to the bonded structure; ε_{crit}, critical strain of the bonded structure; λ, Langrangian operator; ν, Poisson ratio; o_N, normal component of stress; o_{struct}, structural stress distribution in the adhesive layer; o_T, tangential component of stress; $\sum F$, sum of the force due to the applied strain; φ, angle of testing of the Arcan device; γ, semivariogram

1 | INTRODUCTION

Adhesive bonding technology presents several assets compared with classical assembling solutions (eg, riveted, bolted, and welded) such as mass reduction, modularity, and the possibility of joining dissimilar materials. The determination of the strength of adhesively bonded structures is difficult because of the singular stress field at the extremities of the adhesive layer. This stress field mostly depends on the material properties and on the geometry of the bond.[1] Some authors propose closed-form solutions of this stress distribution,[2] which could be used to predict the failure load. However, the applicability of these solutions is often limited to uniaxial loads. It is obvious that for the case of multiaxial loading the stress field along the adhesive layer changes significantly, especially near the singular points. In order to overcome this problem, some other authors propose analytical tools based on experimental test results.[3] An example of software to facilitate the design of adhesively bonded structures can be found in Dragoni et al.[4] In addition, Castagnetti et al[5] proposed the use of finite element modelling by tied mesh method and obtained good results for some complex bonded structures. Some other strategies exist, such as the point stress method,[6,7] which are based on material strength. However, they require an important amount of experimental work to be performed. On the other hand, energetic methods based on fracture mechanics necessitate the existence of a precrack in the structure, which is difficult to take into account during the preliminary design phase.[8] Yet, there is a lack of efficient design tools, as all methods mentioned before are very difficult to be applied for the case of complex geometrical bonded structures. As it has been shown in Leguillon,[9] the combination of both stress and energetic criteria forms the necessary and sufficient condition to predict failure of an adhesively bonded joint. Similar techniques to predict damage initiation and propagation like the cohesive zone model (CZM)[10] also exist; yet these last solutions greatly increase the computational cost and cannot be used in a predimensional phase. All previous methodologies consider the behaviour of the adhesive as linear elastic. Recently, the mathematic behaviour law of a ductile adhesive has been integrated to describe the fracture using CZM,[11] which showed that in this case the fracture toughness G^C is independent of the mode ratio. In the same study, the identification of the parameters of the constitutive response of the cohesive elements has been performed according to classical fracture mechanics tests.[12]

Based on the previous discussions, it is obvious that the design of an adhesively bonded joint is a very complex process. This process can be facilitated when identifying the best concepts among several solutions at the predesign phase. The minimization of the time of this early stage in order to obtain an optimal structure is of great industrial interest. Hence, the use here of complex finite element modelling is inappropriate. The aim of this paper is to propose a tool to be used at the predesign phase of adhesive joints capable to predict the failure load quickly. This tool should be conservative compared with the failure load measured experimentally, capable to predict the tendency when changing the load state and/or the thickness of the adhesive layer, etc, not limited by uniaxial loads and applicable to a wide range geometrical structures. In order to achieve these targets, the coupled stress-energetic criterion[9,13,14] has been chosen. One of the advantages of this criterion is the small experimental campaign required in order to obtain an estimation of the strength of the bonded joint. However, the identification of the stress distribution along the adhesive layer is needed. This can be achieved by means of finite element analysis (FEA)[15]; yet at an increased computational time due to the very fine mesh needed to obtain a proper evaluation of the stress field. Therefore, a sandwich-type model[16,17] is used here. Although these methods have already been published and tested before, their applicability has been demonstrated until now only to classical joint geometries like the single or the double lap joints. In addition, very few data can be found in literature concerning the comparison between experimental and numerical predictions of the previous models.

The first section of this article presents the coupled criterion and shows how it has been implemented with the sandwich-type model (semianalytical approach). An extension of the applicability of this approach to general three-dimensional (3D) structures is also proposed based on spatial interpolation by means of the Kriging method,[18] which is briefly described at the end of the second section. In the third section, FEA and semianalytical predictions are compared with experimental data issued from a double-notched sample tested with the Arcan fixture at various load ratios (tension, shear, and tension/shear). For the case of complex 3D structures, a parametric study would be useful to identify the proper configuration. However, this kind of study would require a huge amount of computational points and should be repetitive. Therefore, in the last part of the article, the application of the surrogated model to dimension a 3D geometry of an adhesive joint using a limited number of calculated points is illustrated.

2 | METHOD

2.1 | Coupled stress-energetic criterion

The application of the coupled stress-energetic criterion requires first a condition for crack onset. For this reason,

a quadratic criterion is used here, which mathematically can be expressed as[13]

$$\sqrt{\left(\frac{\sigma_N(x)}{Z_N}\right)^2+\left(\frac{\sigma_T(x)}{S_C}\right)^2}\geq 1, \tag{1}$$

where σ_N and σ_T are the actual normal and tangential components of the nominal stress, respectively, Z_N and S_C are their corresponding maximums, and x describes the distance from the singular point.

In the general case where the bonded structure is submitted to biaxial loading, the stress state can be described by Equation 2, where only the positive part $\langle\sigma_N(x)\rangle_+$ of the normal stress is taken into account; the compression stresses are supposed to maintain the crack closed.[13] The quantity r^σ defined in Equation 3 is called ratio of multiaxiality.

$$\sigma_{struct}(x)=\langle\sigma_N(x)\rangle_+ +\sigma_T(x) \tag{2}$$

$$r^\sigma(x)=\frac{\sigma_N(x)}{\sigma_{struct}(x)} \tag{3}$$

Introducing Equations 2 and 3 in (1) permits to write

$$\sigma_{struct}(x)\sqrt{\left(\frac{r^\sigma(x)}{Z_N}\right)^2+\left(\frac{1-r^\sigma(x)}{S_C}\right)^2}\geq 1. \tag{4}$$

In order to solve the coupled criterion, it is convenient to introduce a dimensionless variable $k_{struct}(x)$ to characterize the stress field in the adhesive layer. Therefore, $\sigma_{struct}(x)$ can be written as[13]

$$\sigma_{struct}(x)=k_{struct}(x)\cdot E^{eq}\cdot\varepsilon, \tag{5}$$

where ε is the strain applied to the structure and $E^{eq}=E/(1-\nu^2)$ is an equivalent modulus of the adhesive under plane strain hypothesis. It is obvious that the stress criterion expressed by Equations 4 and 5 is fulfilled for an internal length $x=a_\sigma$ (Figure 1A).

As it was discussed in the introduction part, the necessary and sufficient condition to predict the failure of adhesively bonded joints needs also the determination of an energetic criterion to describe crack propagation. It is well known from the fracture mechanics theory that crack propagation takes place once the potential energy introduced in a solid medium becomes grater or equal to G^C. Mathematically, for the case of adhesives, this principle can be expressed as

$$G_{inc}(a)=-\frac{W_p(a)-W_p(0)}{\Delta S}\geq G^C(a), \tag{6}$$

where the cracked surface is denoted as ΔS, and $W_p(0)$ and $W_p(a)$ are the global potential energies of the structure at the initial 0 and cracked a states, respectively. It must be mentioned here that the crack propagation is simulated by several linear elastic calculations for incremental values of the crack length. Therefore, G_{inc} is used in Equation 6 to account for the incremental strain energy release rate. The energy criterion is fulfilled for a certain value of the crack length $a=a_{en}$ (Figure 1B).

Similarly to the stress criterion, a dimensionless parameter $A_{inc}(a)$ can be introduced to describe the evolution of G_{inc}. This parameter will also be used later on to solve the coupled criterion. Thus, G_{inc} can also be expressed as[13]

$$G_{inc}(a)=A_{inc}(a)\,.\,E^{eq}\,.\,\varepsilon^2\,.\,t\geq G^C(a), \tag{7}$$

where t is the adhesive joint thickness.

According to Equations 5 and 7, a schematic representation of the evolutions of the stress and the energy release rate as a function of the distance from the singular point is shown in the following figure.

The solution of the coupled criterion assumes that fracture initiates once both the stress and energetic criterions are satisfied simultaneously for an internal length a^*. If the geometry is modelled with finite elements, a linear elastic simulation with no crack permits to calculate $k_{struct}(x)$. On the other hand, several linear elastic calculations for different values of the crack length are needed to compute $A_{inc}(a)$. At the critical point where $x=a=a^*$, the applied strain ε predicted by both the stress and energetic criteria is also the same. Therefore, by combining Equations 4, 5, and 7, a^* is the solution of the following equation:

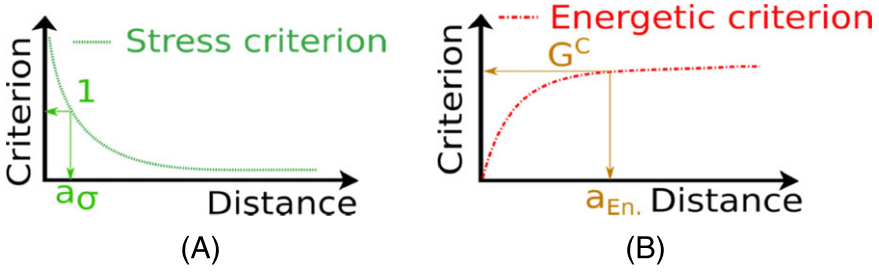

FIGURE 1 Evolutions of A, the stress and B, the energy release rate as a function of the distance from the singular point, showing also the characteristic value of the internal length where each of the criterions are fulfilled [Colour figure can be viewed at wileyonlinelibrary.com]

$$\frac{L^C(a^*)}{t} = \frac{A_{inc}(a^*)}{[k_{struct}(a^*)]^2}, \tag{8}$$

where $L^C(a^*) = E^{eq} \cdot G^C(a^*) \left[\left(\frac{r^\sigma(a^*)}{Z_N} \right)^2 + \left(\frac{1-r^\sigma(a^*)}{S_C} \right)^{2.} \right]$.

The quantity L^C has length units and can be considered as a characteristic length of the joint. Finally, after reading in the finite element model the sum of the forces applied on the structure $\sum F$, the failure load $F^{fail.}$ is simply computed by means of the equation below[9,15]:

$$F^{fail.} = \sum F \cdot \varepsilon_{crit}, \tag{9}$$

where ε_{crit} is the critical strain computed from either the stress or the energetic criterions at $x = a = a^*$.

2.2 | Implementation of the coupled criterion

In the present work, two ways of implementing the coupled criterion are examined. The first method makes use of the FEA as described in Leguillon[9] and Carrere et al[13] and the second one of an analytical model in order to minimize the computational cost. The analytical model chosen here is the sandwich-type model initially developed by Bigwood and Cromcombe[16] and modified later on by Weißgraeber et al,[17] where the stresses and strains in the substrates are described according to the first order shear deformation theory. The section forces required in this closed-form solution are evaluated from the global structure as shown in Figure 2. The extremities of the joint are named with i,j indexes, where $i = 1$ corresponds to the upper and $i = 2$ to the lower adherent; the second index j denotes the left ($j = 1$) and right ($j = 2$) sides of the joint. In Figure 2C, N_{ij}, T_{ij}, and M_{ij} represent the normal, tangential, and bending moment components of the sections forces, respectively.

Once the section forces are measured from a poorly meshed FEA model as shown in Figure 2, the stress distribution inside the adhesive and at the adhesive/substrate interface is determined according to the analytical model of Weißgraeber.[17] Afterwards, the stress-based criterion is applied as discussed in Section 2.1. However, the application of the energy-based criterion with the semianalytical approach is more complicated. First, the crack propagation is considered as equivalent to a reduction of the bonded length, as presented in Figure 3.

The stress distribution is given by the sandwich-type model[17,19] for the remaining bonded length denoted as $\widetilde{L} = L_{rc} - a$. Based on the maximum values of the normal and shear stresses (σ_{max} and τ_{max}, respectively) extracted for $\widetilde{L}$, the energy release rate $G_{SA}(a)$ is computed according to the following equation[14,20]:

$$G_{SA}(a) = \frac{t}{2E_a} \cdot {\sigma_{max}}^2 + \frac{t}{2G_a} \cdot {\tau_{max}}^2, \tag{10}$$

where E_a and G_a represent the Young's and Shear modulus of the adhesive, respectively. Then, $G_{inc}(a)$ is

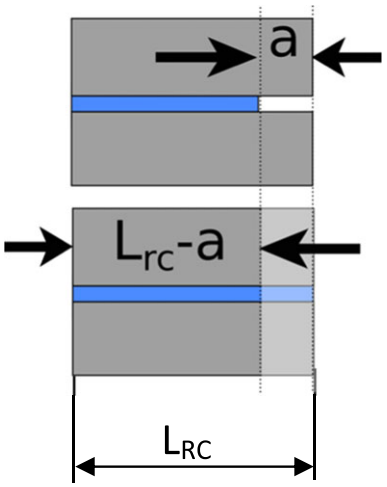

FIGURE 3 Simulation of the crack propagation with the semianalytical approach [Colour figure can be viewed at wileyonlinelibrary.com]

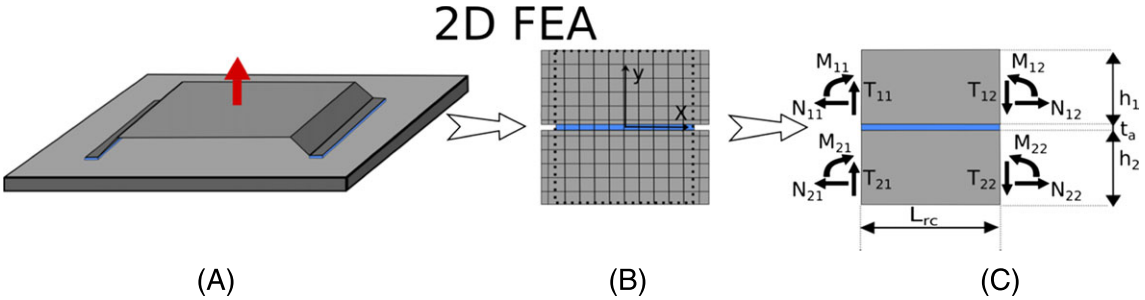

FIGURE 2 Schematization of the semianalytical approach from A, the global three-dimensional (3D) structure, B, reduced to a two-dimensional (2D) finite element analysis (FEA) model, and C, extraction of the section forces to use with the Weißgraeber[17] model [Colour figure can be viewed at wileyonlinelibrary.com]

calculated by integrating $G_{SA}(a)$ along the considered crack length a as shown in Equation 11, and the dimensionless coefficient $A_{inc}(a)$ can be extracted by means of Equation 7 as explained before in Section 2.1.

$$G_{inc}(a) = \frac{1}{a}\int_0^a G_{SA}(a)da,\ 0 \le a \le a^* \tag{11}$$

It must be mentioned here that the FEA method can give access to the evolution of the mode ratio during crack propagation.[13] However, this is not possible with the semianalytical approach; in this case, the mode ratio is supposed constant. Therefore, in Equation 7, $G^C(a) = G_I^C$ or G_{II}^C (the fracture toughness under pure mode I or II load, respectively) according to the loading and crack propagation modes.

2.3 | Surrogated model

As it was discussed in Section 1, in case of complex 3D joint geometries, the consideration of the influence of certain parameters (eg, length and/or width of the adhesive layer, thickness of the adhesive and/or the substrates, etc) in the failure load of the structure is indispensable during the design phase, mainly when performing optimization loops. This would require a parametric study and the methodology previously presented would have to be applied for a huge amount of points. It is obvious that this is impossible to realize in an industrial environment. In such cases, it is compulsory to estimate the behaviour of the overall structure using a limited number of known points.[18,21] This can be achieved by means of spatial interpolation using an appropriate statistical tool. In the present paper, the Kriging model[22] is chosen, and it will be briefly presented in this section.

Let f be the mathematic image of an entire response surface constructed by P_i ($i = 1$ *to* m) points lying on the x-y plane ($P_i = (x,y)$). The main idea is to estimate the form of the function f on a certain number of points P_u ($P_u \neq P_i$) from the known values of f in P_i, using the following equation:

$$f(P_u) = \sum_{i=1}^{m} W_i \cdot f(P_i). \tag{12}$$

Therefore, the problem consists of determining the appropriate weight values W_i on each of the environmental points P_i. According to the Kriging method, these values of W_i are chosen based on the distance of the points P_i from the point P_u where f is to be defined, as it is explained in Bachoc.[23] At first, the semivariogram $\gamma(h)$ is calculated, which in its general form for a number of points $n(h)$ separated by a distance $h = |x_i - y_i|$ can be expressed by the following equation:

$$\gamma(h) = \frac{1}{2 \cdot n(h)} \sum_{i=1}^{n(h)} (x_i - y_i)^2. \tag{12}$$

Adjusting an analytical function for $\gamma(h)$ by means of the least squares method permits to completely characterize the semivariance as a function of the distance between the environmental points. The correct choice of this function is the key issue of the Kriging method. An extended discussion on the different types of variogrammes and of their behaviour can be found in other studies.[23,24]

The last step consists of calculating the weights W_i of Equation 12. Here, several solutions can be found in literature; for the needs of the present study, the most common one called ordinary Kriging is used.[23] According to ordinary Kriging, the set of weights W_i should guarantee that the value of the estimated function of the semivariogram calculated using the target point P_u will rely on the curve defined in the previous step by means of the least squares method. In Equation 13, the m semivariances associated at each one of the m known points P_i are represented by the lines of matrix A; these values are computed based on the distance between these points. The lines of vector $\boldsymbol{B}$ correspond to the values of the semivariogram at the target point P_u, which are calculated by means of the analytical function of γ. Therefore, the set of weights W_i is the solution of a system of $m + 1$ linear equations with $m + 1$ unknown variables,[23] which can be solved simply by inversing matrix A. In order to obtain a non-biassed solution, the sum of the weights W_i has to be equal to 1. This adds a supplementary degree of freedom in the problem, which is taken into account by means of the Langrangian operator λ in the last line of vector $\boldsymbol{W}$ in Equation 13, and is used to minimize the error of the solution.[23]

$$A \cdot W = B, \tag{13}$$

$$\text{where } A = \begin{bmatrix} \gamma(h_{11}) & \gamma(h_{12}) & \cdots & \gamma(h_{1m}) & 1 \\ \gamma(h_{21}) & \gamma(h_{22}) & \cdots & \gamma(h_{2m}) & 1 \\ \vdots & \vdots & \ddots & \vdots & \vdots \\ \gamma(h_{m1}) & \gamma(h_{m2}) & \cdots & \gamma(h_{mm}) & 1 \\ 1 & 1 & \cdots & 1 & 0 \end{bmatrix},$$

$$\boldsymbol{W} = \begin{bmatrix} \boldsymbol{W_1} \\ \boldsymbol{W_2} \\ \vdots \\ \boldsymbol{W_m} \\ \boldsymbol{\lambda} \end{bmatrix} \text{ and } \boldsymbol{B} = \begin{bmatrix} \boldsymbol{\gamma(h_{1u})} \\ \boldsymbol{\gamma(h_{2u})} \\ \vdots \\ \boldsymbol{\gamma(h_{mu})} \\ \boldsymbol{1} \end{bmatrix}.$$

The Kriging method can also provide the variance of the estimation. This is described by the squared standard error deviation S_p at each one of the computed points of the response surface, which can be obtained by means of Equation 14. Therefore, the probability that the real solution is in the confidence interval of $f(P_u) \pm S_p$ is 68%, at $f(P_u) \pm 2S_p$ is 95%, etc, (see Bachoc[23]):

$$S_p^2 = W^T.B. \tag{14}$$

The aim is to compute the response surface by only using a few points in the range of the studied parameter. According to other studies,[18,25] the implementation of the Kriging method is composed of four stages described in the following list:

- Stage 1: Normalization of the studied parameter range, in order to obtain a set of values in the [−1, +1] interval. This step, is only used to make parameters discretization easier. In the end, this normalized range is converted to the real parameter range;
- Stage 2: Realization of a number of computations to determine the model response on a certain number of points. These calculations are inevitable; yet, regarding the computational cost, this stage is the most expensive one.
- Stage 3: Interpolation according to the Kriging method on a certain number of points where the response of the model is unknown, in order to obtain the response surface;
- Stage 4: Estimation of the reliability of the response surface obtained in stage 3, by computing the standard error deviation of the solution using Equation 14.

3 | APPLICATIONS

3.1 | Experimental validation on a double-notched specimen

3.1.1 | Materials and bonding procedure

In order to test the methodology previously presented, a bi-component adhesive (Loctite Hysol EA 9395 commercialized by Henkel) was preferred due to its strong fragile behaviour.[26,27] This is essential since the coupled criterion does not take into account material non-linearity, which is very pronounced for the case of ductile adhesives. The resin and the crosslinking agent were mixed at a ratio of 100:17 g, as also recommended in the datasheet of the adhesive, by means of a speed-mixer machine (DAC 150.1 FV-K) in order to obtain a homogenous mixture. The adherents were made from 2017A aluminium alloy; they were cleaned prior to bonding by immersion into pure 99% acetone for 2 hours and then dried in an oven at 120°C for 1 hour. The surfaces of the substrates to be bonded were prepared mechanically by grinding with SiC paper (grade 180). Any final remaining due to this procedure were simply wiped off by means of pure 99% acetone. The thickness of the joint was set at 0.4 mm. The adhesive was applied on both substrates manually with a spatula at ambient conditions (20°C and 50% of relative humidity). In order to guarantee proper alignment and good repeatability of the thickness at a tolerance of ±0.05 mm, a special system similar to the one shown previously in Badulescu et al[28] was used to perform the bond. The assembled specimens were cured at 76°C for 90 minutes. The experiments were performed using a universal tensile machine. The samples were tested under displacement control, at a loading rate of 0.5 mm/min also at ambient conditions (20°C and 50% of relative humidity). Table 1 shows the mechanical properties of the adherents and the adhesive; the failure stresses Z_N and S_C are estimated from the average failure stresses.[28,29]

3.1.2 | Arcan device

The experiments were performed by means of the modified Arcan fixture,[30] which was chosen due to its ability to generate different load states on the adhesive layer as it will be explained below. Figure 4A shows the geometry of the substrates (see Table 2); the holes were drilled in order to facilitate the mounting of the specimen on the Arcan device. The presence of beaks strongly reduces stress concentration at the front and back sides of the joint.[30,31] Therefore, crack initiation and propagation is expected to occur from the extremities of the adhesive layer. A schematization of the final geometry of the bonded specimen is given later on in Figure 6. A general overview of the modified Arcan set-up that was used to perform the tests with a specimen fixed on it, is given in Figure 4B. The

TABLE 1 Mechanical properties of the adherents and the adhesive

	Modulus, GPa	Poisson Ratio	G^C Mode I, J/m^2	G^C Mode II, J/m^2	Z_N, MPa	S_C, MPa
Hysol© EA 9395	5.0	0.35	191.0 ± 7.2 (Jumel et al[26])	130 < G^C < 275 (Salem et al[27])	26.1 ± 4.3	46.7 ± 8.2
Aluminium 2017	70.0	0.33	/	/	/	/

/, Gc mode I, II and the parameter Zn and Sc are not used for the aluminium adherent.

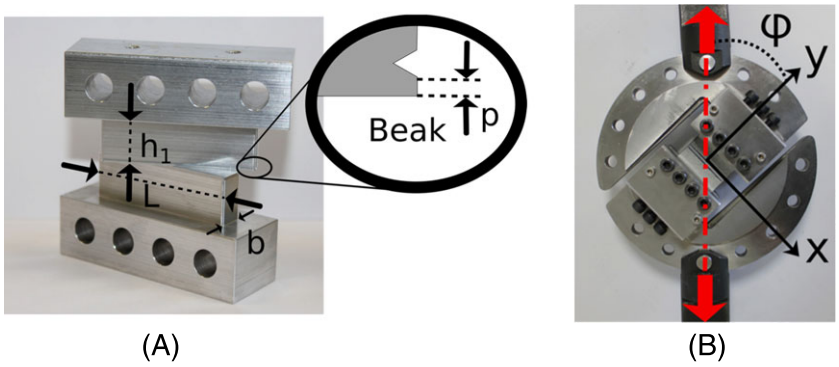

FIGURE 4 Modified Arcan device: A, Geometry of the substrates. B, General overview of the set-up with the mounted specimen [Colour figure can be viewed at wileyonlinelibrary.com]

TABLE 2 Characteristic dimensions of the substrates

	Dimension, mm
L	50
h_1	15
b	9.5
p	0.2

connection with the tensile machine is achieved via the loading pins. According to Figure 4B, the x-axis points towards the direction of the adhesive layer and the y-axis towards the out-of-plane direction. Hence, the modified Arcan fixture permits to vary the angle φ between the y-axis and the loading axis from 0° (pure out-of-plane tension) to 90° (pure in-plane shear) and 135° (combined out-of-plane compression/in-plane shear), with a step of 22.5°. As it was previously discussed, in the method of implementation of the coupled criterion that was adopted in the present study, only tensile and shear loads are considered to allow crack propagation. Therefore, three values of the angle φ were tested: 0°, 45°, and 90°.

3.1.3 | Double-notched sample

The Arcan substrates that are used to identify the behaviour law of an adhesive have a special geometry to reduce the edge effects (beaks[30] in Figure 5). However, as it was previously discussed, adhesively bonded structures used in industry strongly suffer from stress concentrations at the extremities of the joint. In addition, the application of the coupled criterion requires a stress singular point to simulate crack initiation and propagation. Therefore, during the preparation of the Arcan specimens, two notches of 5 mm of length were created at each one of the extremities of the joint, thus resulting to the so called double-notched specimen (DNS) geometry. A schematic representation of the DNS geometry is given in the following figure.

Three tests per each phase angle (0°, 45°, and 90°) were performed. The measured force-displacement curves are presented in Figure 6. The normal force (NF) vs the normal displacement (ND) is plotted at 0°; at 90°, the tangential force (TF) vs the tangential displacement (TD) is shown. The normal and tangential directions are named with respect to the adhesive layer. It is obvious that for the case of 45°, the NF and TF components used in the graphs correspond to the experimentally measured force multiplied by $\sqrt{2}/2$. At all phase angles, the components of the displacement were determined by digital image correlation using the Aramis GOM 4M system, which allows to measure the relative displacement between the two substrates close to the adhesive layer. The results show that the adhesive has a brittle behaviour at 0°, with the breaking force being slightly above 10 kN. Similar behaviour for both the normal and the tangential components of the displacement has also been measured at 45°, with the failure load being slightly below 10 kN. The

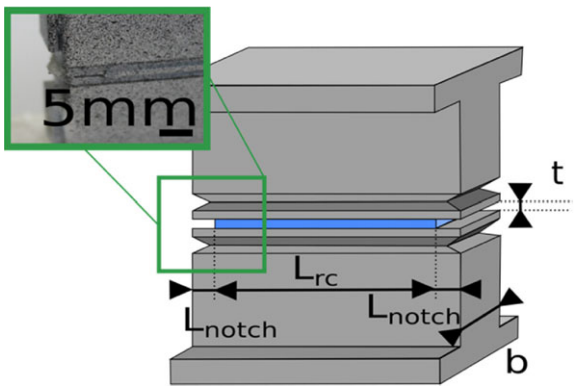

$$L_{rc} = 40\ mm$$

$$L_{notch} = 5\ mm$$

$$t = 0.4\ mm$$

$$b = 9.5\ mm$$

FIGURE 5 Double-notched sample [Colour figure can be viewed at wileyonlinelibrary.com]

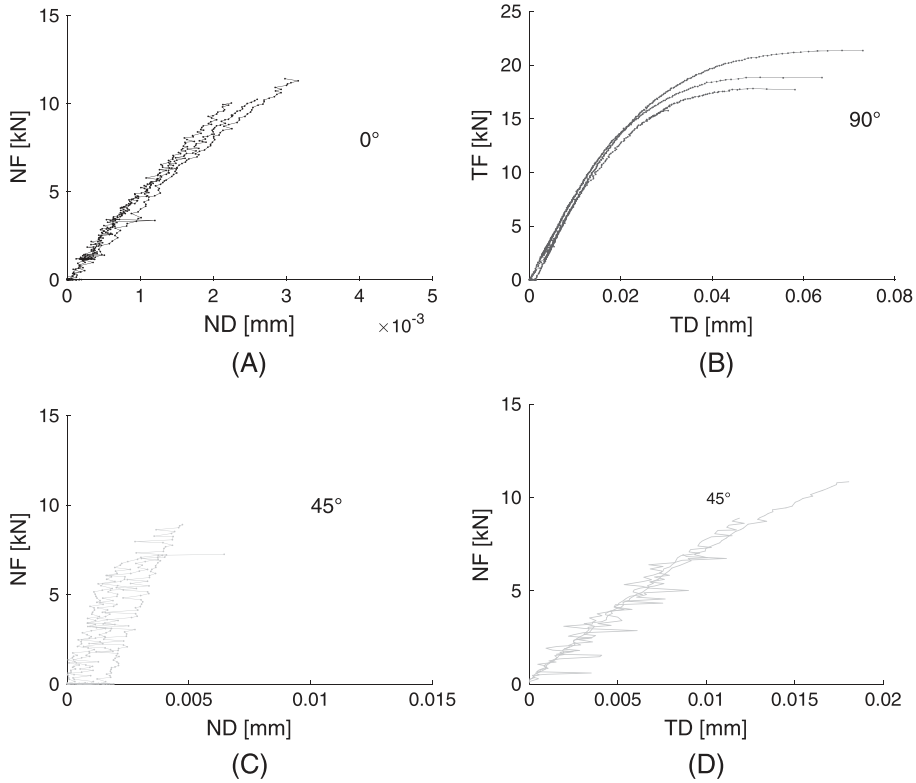

FIGURE 6 Force/displacement curves at (A) 0°, (B) 90°, (C) 45°, NF vs ND, and (D) 45°, TF vs TD. ND, normal displacement; NF, normal force; TD, tangential displacement; TF, tangential force

shear test puts in evidence a non-linear behaviour of the adhesive joint; the force at rupture was measured here between 15 and 25 kN.

3.2 | Numerical

The experimental values of the NF as a function of TF at failure for the 3 phase angles tested are plotted in Figure 9. The predictions of the failure load by means of the coupled criterion applied with finite elements and with the semianalytical approach are also added in the graph. All results are presented using the mean value ± the standard deviation.

Looking at the results in Figure 7, it can be concluded that the FEA predictions are in good agreement with the experimental measurements. Concerning the semianalytical approach, the estimation of the failure load is conservative compared with the experimental data; this difference could be partially attributed to the mode ratio which is supposed constant in this case as it was discussed in Section 2.2. It is obvious that this is not true for the total duration of each test. For instance, low levelled mode II and mode I components of the load are also introduced during the tensile and shear tests, respectively, due to the deformation of the substrates;

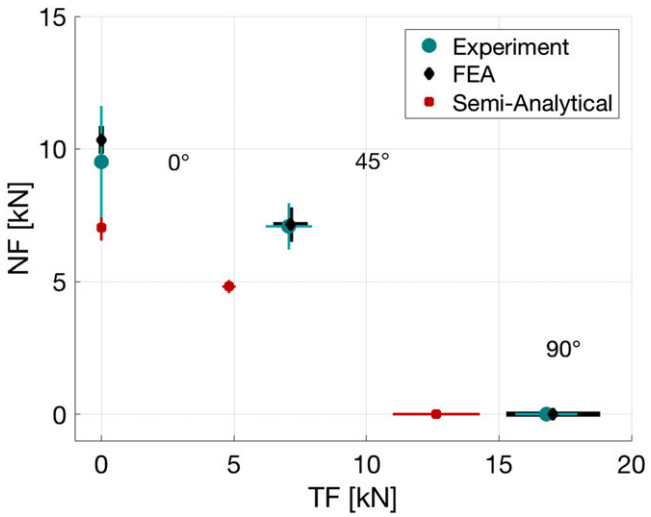

FIGURE 7 Comparison of the experimental failure load and the numerical prediction. FEA, finite element analysis; NF, normal force; TF, tangential force [Colour figure can be viewed at wileyonlinelibrary.com]

these components cannot be taken into account with the semianalytical approach. In addition, the stress distribution along the adhesive layer obtained from the closed-form model presents a high difference with the one obtained by FEA. An example is given in Figure 8 for the case of 0° phase angle: the normal stress

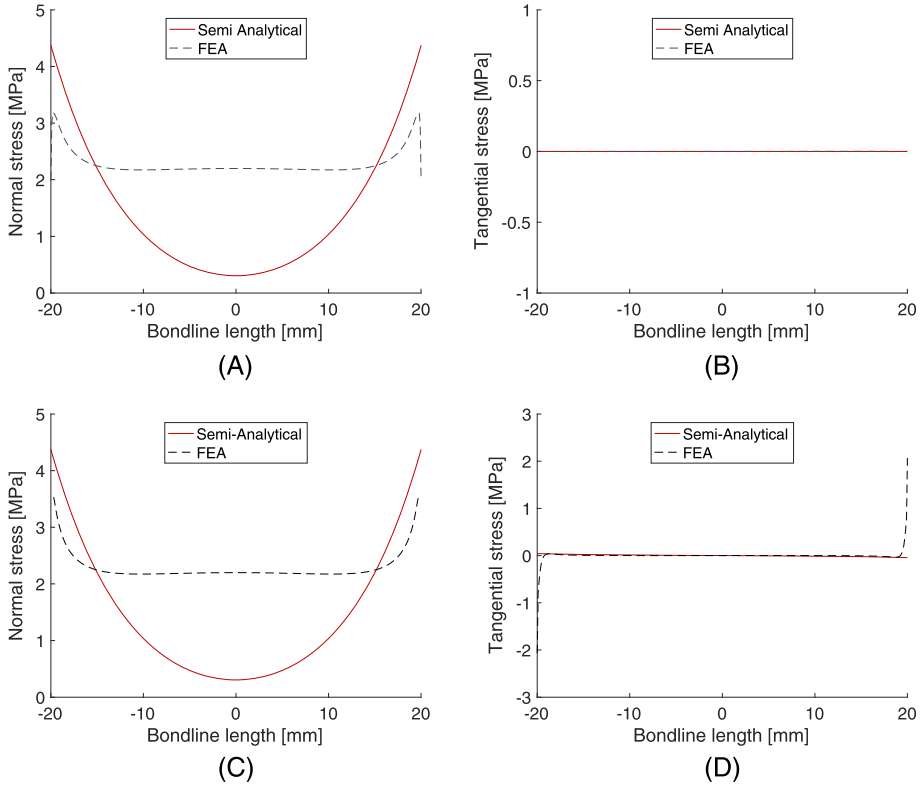

FIGURE 8 Stress distribution along the adhesive layer for the DNS Arcan specimen loaded at 0°: A and B, Mid-thickness of the bond line. C and D, Adhesive/substrate interface [Colour figure can be viewed at wileyonlinelibrary.com]

distribution given by the sandwich-type model of Weißgraeber[17] compared with FEA is overestimated at the extremities and underestimated at the centre of the bond line, for both the middle of the adhesive layer thickness and the adhesive/substrate interface (Figure 8A,C, respectively). On the other hand, the tangential stress predicted by the Weißgraeber model[17] is zero for the two previous cases (Figure 8B,D), which is not the case at the two extremities of the adhesive layer when examining the tangential stress field given by the FEA model at the interface of the joint (Figure 8D). Besides these differences, the conservative predictions of the semianalytical approach show the reliability of the use of this methodology in the predimensional phase of adhesively bonded structures. In addition, the tendency in the evolution of the failure load is also respected, as it is shown by the graph in Figure 7. It must be mentioned here that the semianalytical approach reduced the computational cost by a ratio of 750 compared with the FEA model as it is presented in Figure 9. This is due to the fact that in this case no fine mesh is required around the singular area and/or along the thickness of the adhesive layer (as also discussed in the previous sessions).

Even though the aim of the paper is to propose a tool based on a closed-form solution to estimate the failure load of adhesively bonded joints in order to avoid numerical

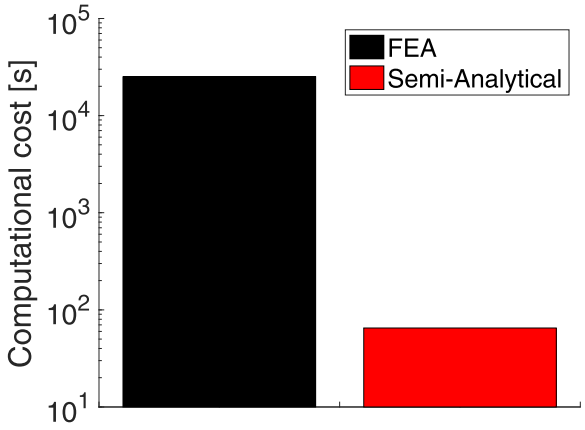

FIGURE 9 Comparison of the computational cost between finite element analysis (FEA) and semianalytical approach [Colour figure can be viewed at wileyonlinelibrary.com]

modelling of the structure, it is convenient here to make a brief discussion on the influence of the mesh size in the predictions of the failure load of the coupled criterion when FEA is used. Therefore, Figure 10A,B presents the evolutions of the failure load and the internal length a^*, respectively, as a function of the number of elements along the adhesive layer thickness, calculated after application of the coupled criterion by means of FEA for the 0° phase angle. The graphs show a clear influence of the mesh size:

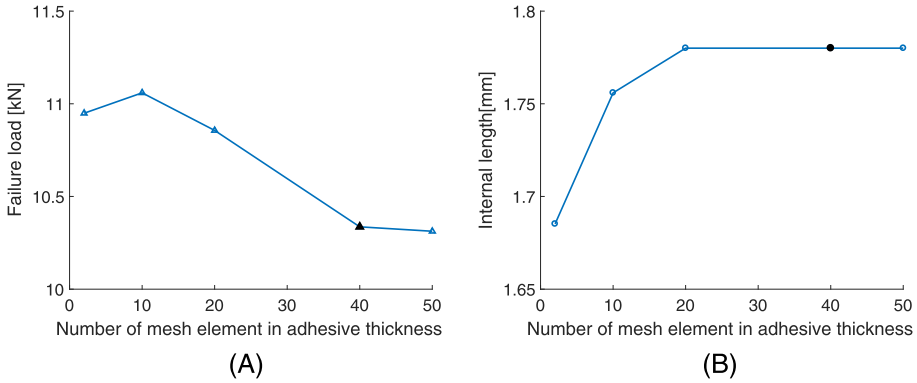

FIGURE 10 Influence of the mesh size on A, the failure load and B, the internal length determined by the coupled criterion after numerical modelling of an Arcan specimen loaded at 0° [Colour figure can be viewed at wileyonlinelibrary.com]

a^* converges to 1.78 mm after using 20 elements or more. On the other hand, the failure load converges to the value of 10.35 kN for a number of elements equal to 40 or higher. It must be mentioned here that the response of the coupled criterion by means of numerical modelling of the bonded structure has been the subject of other research teams too in the past, mainly for the case of the single lap joint (SLJ) geometry.[13,14,32,33] The authors in Carrere et al[13] and Moradi et al[32] recommended 40 elements along the adhesive thickness in order for convergence to be achieved. Similar conclusions were observed when also studying the SLJ in the present research too, which are not presented here in order to avoid unnecessary repetitions. Therefore, according to all these results, 40 elements were used along the adhesive layer thickness for the FEA of the Arcan tests to predict the failure load at all the phase angles examined experimentally in this study.

3.3 | Response surface of the failure load of a bonded structure

Design is an iterative process; each loop tends to converge towards the final configuration. The previous section presented a solution able to decrease the computational cost for a single loop. As presented for the DNS sample, an asymptotic stress field due to the edge effects exists at the extremities of the bond line. However, the global geometry of the structure can also have an impact on the stress distribution (see Table 3). Therefore, a parametric study is compulsory to determine the best configuration. This section presents a method to build efficiently a response surface by means of spatial interpolation using the Kriging model.[18]

A bonded plateau representative of an industrial application has been chosen for the demonstration (Figure 11). Both adherents are supposed of aluminium alloy, and the upper part of the structure is submitted to a unit load along the y-direction. The influence of the thickness of the upper adherent (t_{ext}) and of the bonded length (L_{rc}) on the failure load of this assembly have been investigated (Table 3).

TABLE 3 Characteristic values of the dimensions of the bonded plateau

	Dimension, mm
$L1_{Plate}$	50
$L2_{Plate}$	50
L_{Sub_inf}	15
H_{Plate}	15
t_{adh}	15
t_{ext}	5-10
L_{rc}	9-25

For a certain number of points in the range area of the studied parameters, the section forces are estimated on a poorly mesh FEA model of the bonded structure (as discussed in the previous sessions), and the failure load is determined with the same methodology as described above for DNS Arcan specimen. The results obtained with this method are represented with the black spots in Figure 12, and the response surface is estimated according to the Kriging method (coloured surface, Figure 12A).

The error associated to the response surface is presented in Figure 12B. The maximal error is observed at the (red) area where the density of calculated points is the lowest. It is obvious that the quality of the response surface is directly related to the number of the starting (black) points. In order to justify the amount of calculated points used to construct the response surface, several techniques can be found in literature.[24] The best solution would be to calculate all the points of the response surface and compare with the Kriging method predictions. However, this requires a huge amount of computations to be performed. Another solution would be to calculate

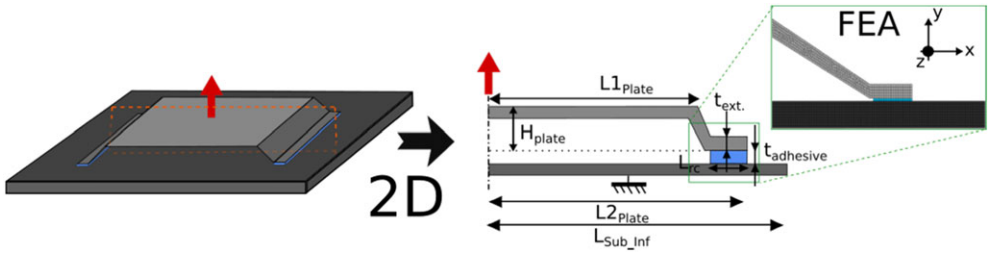

FIGURE 11 Schematization of the bonded structure and simplification in two-dimensional (2D) in order to perform the optimization loop. FEA, finite element analysis [Colour figure can be viewed at wileyonlinelibrary.com]

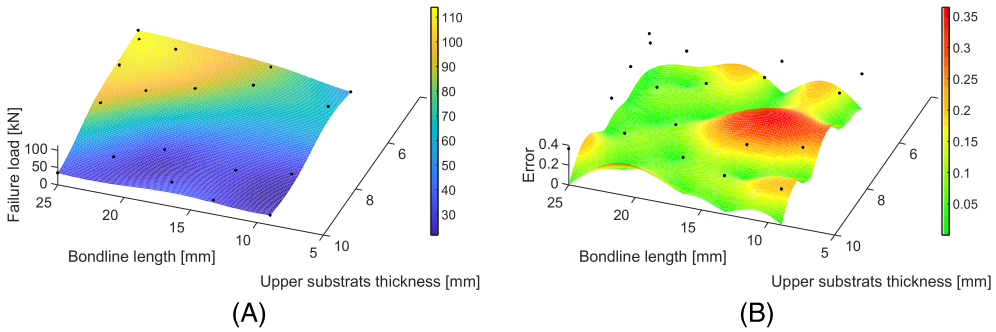

FIGURE 12 A, Response surface obtained with Kriging method. B, The associated error [Colour figure can be viewed at wileyonlinelibrary.com]

some additional starting points, build a new response surface and compare with the previous one. Unfortunately, the computational cost of this second solution is also very high. Therefore, the strategy chosen in this study is the Leave-and-Out method[34] (Figure 13). Basically, the first response surface is obtained with a certain number of starting points; then a second one is obtained with a reduced amount of starting points. The interpolated values (response surfaces) are compared and the process is repeated until the error of the estimation is minimized. Figure 14 shows the comparison between the computed (starting) points obtained from the coupled stress-energy criterion and those obtained from the spatial interpolation when using the Leave-and-Out method. It is obvious that by increasing the number of points involved in the identification process, the spatial correlation error will decrease. However, in terms of the computational cost, the Leave-and-Out techniques provide information on the quality of the interpolation.

The interpolated surface tends to overestimate the low failure load values and underestimate the higher ones (see Figure 14B,C), which is difficult to observe for a low amount of starting points (Figure 14A). In addition, by increasing the amount of starting points the response surface adjusts well with the computed points (as expected). In the present case, the target is to obtain the optimal values for the thickness t_{ext} and the length L_{rc} (Figure 11; Table 3), in order for the bonded structure to have the best resistance to the external load. Looking at Figure 14, the response surface obtained from the 20

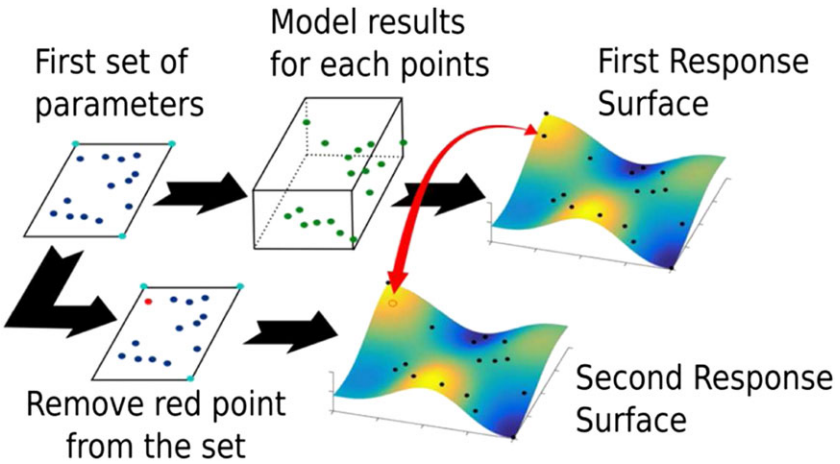

FIGURE 13 Illustration of the Leave-and-Out technique[34] to assess the reliability of the interpolated response surface [Colour figure can be viewed at wileyonlinelibrary.com]

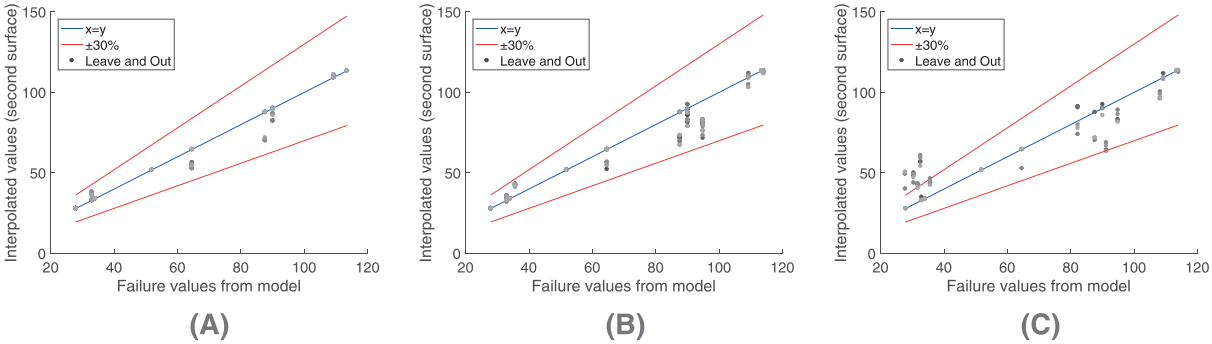

FIGURE 14 Leave-and-Out comparison between the failure model response and the equivalent interpolated values for A, 9 points, B, 12 points, and C, 20 points [Colour figure can be viewed at wileyonlinelibrary.com]

starting points is expected to have the most reliable results. According to the response surface, the best result for the bonded joint of Figure 11 has been obtained for $L_{rc} = 25$ mm and $t_{ext} = 5$ mm. This type of application of the Kriging method is interesting for the predesign phase of adhesively bonded structures, since it reduces considerably the computational time of the virtual design loops required to obtain the optimal solution.

4 | CONCLUSIONS AND PERSPECTIVES

In this paper, a strategy to predict the strength of an adhesively bonded structure is proposed. The methodology uses intrinsic values for the properties of the adhesive such as the failure stress and the fracture toughness under pure mode I and II loads. These properties are inserted in a coupled stress—energetic criterion, which forms the necessary and sufficient condition to predict the strength of an adhesive joint. Crack onset is based on the predictions of a quadratic stress criterion. Crack propagation is modelled according to the Linear Elastic fracture mechanics theory. Failure occurs once both the stress and energetic criterions are fulfilled at a certain distance from the singular point called internal length. In order to avoid very fine meshes and reduce the computational cost, a previously published closed-form solution is used to represent the asymptotic stress field along the adhesive layer. The predictions of the failure load of this semianalytical approach were found conservative compared with the experimental results and the finite element calculations for the case of a double-notched Arcan specimen at all load ratios examined. In addition, the tendency of the evolution of the failure load as a function of the mode ratio could also be described. Moreover, it has been shown that the semianalytical approach reduced the computation time by a factor of 750 compared with FEA. The application of the methodology has also been extended to 3D structures by means of spatial interpolation using the Kriging model. Finally, an optimization method for the critical geometric quantities of an adhesively bonded structure is proposed, based on the quality of the interpolation as calculated by the Leave-and-Out technique. All these solutions should be useful for researchers and/or engineers at the predesign phase of adhesive joints.

As a first perspective to the current work, it can be mentioned the prediction and comparison with experimental data of the failure loads of adhesive joints submitted to complex load states (combinations of tension, shear, torsion, and compression loads). Furthermore, the validity of the strategy presented here should also be extended for ductile (eg, crush-optimized) adhesives too, by taking into account their non-linear behaviour. In addition, it is of great interest to examine the applicability of the methodology on axisymmetric (eg, tubular) joints, since such types of geometries are more and more used in real industrial applications. Finally, it would be also important to look at the possibility of taking into account the friction between the crack faces when under pure shear load, as this has been identified in the past as one of the main sources for higher mode II fracture energies. Some of these aspects are currently being under investigation.

ACKNOWLEDGEMENT

The authors would like to thank ArianeGroup for the financial support of this study.

ORCID

Jérémy Le Pavic http://orcid.org/0000-0002-9788-4257

REFERENCES

1. Bogy DB, Wang KC. Stress singularities at interface corners in bonded dissimilar isotropic elastic materials. *Int J Solids Struct*. 1971;7(8):993-1005.
2. Lazzarin P, Quaresimin M, Ferro P. A two-term stress function approach to evaluate stress distributions in bonded joints of different geometries. *J Strain Anal Eng Des*. 2002;37(5):385-398.

3. Goglio L, Rossetto M, Dragoni E. Design of adhesive joints based on peak elastic stresses. *Int J Adhes Adhes*. 2008;28(8):427-435.
4. Dragoni E, Goglio L, Kleiner F. Designing bonded joints by means of the JointCalc software. *Int J Adhes Adhes*. 2010;30(5):267-280.
5. Castagnetti D, Dragoni E, Spaggiari A. Failure analysis of complex bonded structures: experimental tests and efficient finite element modelling by tied mesh method. *Int J Adhes Adhes*. 2011;31(5):338-346.
6. Whitney J, Nuismer RJ. Stress fracture criteria for laminated composites containing stress concentrations. *J Compos Mater*. 1974;8(3):253-265.
7. Whitworth HA, Aluko O, Tomlinson NA. Application of the point stress criterion to the failure of composite pinned joints. *Eng Fract Mech*. 2008;75:1829-1839.
8. Chen Z, Adams RD, Lucas FM. International journal of Adhesion & Adhesives the use of the J -integral vector to analyse adhesive bonds with and without a crack. *Int J Adhes Adhes*. 2011;31(1):48-55.
9. Leguillon D. Strength or toughness? A criterion for crack onset at a notch. *Eur J Mech a/Solids*. 2002;21(1):61-72.
10. Pirondi F, Guiliese G, M F. Development of a cohesive zone model for three-dimensional simulation of joint de-bonding/ delamination under mixed-mode I/II fatigue loading. *Int J Struct Integr*. 2014;5(3):171-186.
11. Stamoulis G, Carrere N. Investigating the influence of material non-linearity in the fracture properties of ductile adhesives submitted to mixed-mode loading. *Eng Fract Mech*. 2017;179:260-271.
12. Stamoulis G, Carrere N, Cognard JY, Davies P, Badulescu C. On the experimental mixed-mode failure of adhesively bonded metallic joints. *Int J Adhes Adhes*. 2014;51:148-158.
13. Carrere N, Martin E, Leguillon D. Comparison between models based on a coupled criterion for the prediction of the failure of adhesively bonded joints. *Eng Fract Mech*. 2015;138:185-201.
14. Hell S, Weißgraeber P, Felger J, Becker W. A coupled stress and energy criterion for the assessment of crack initiation in single lap joints: a numerical approach. *Eng Fract Mech*. 2014;117:112-126.
15. Moradi A, Leguillon D, Carrère N. Influence of the adhesive thickness on a debonding—an asymptotic model. *Eng Fract Mech*. 2013;114:55-68.
16. Bigwood DA, Crocombe AD. Elastic analysis and engineering design formulae for bonded joints. *Int J Adhes Adhes*. 1989;9(4):229-242.
17. Weißgraeber P, Stein N, Becker W. A general sandwich-type model for adhesive joints with composite adherends. *Int J Adhes Adhes*. 2014;55:56-63.
18. Carrere N, Rollet Y, Leroy F, Maire J. Efficient structural computations with parameters uncertainty for composite applications. *Compos Sci Technol*. 2009;69(9):1328-1333.
19. Weißgraeber P, Becker W. Finite fracture mechanics model for mixed mode fracture in adhesive joints. *Int J Solids Struct*. 2013;50(14-15):2383-2394.
20. Krenk S. Energy release rate of symmetric adhesive joints. *Eng Fract Mech*. 1992;43(4):549-559.
21. Huchet Q, Mattrand C, Beaurepaire P, et al. Cost effective strategy using Kriging surrogates to compute fatigue at multiple locations of a structure: application to offshore wind turbine certification AK-DA. *MATEC Web Conf Fatigue*. 2018;165:1-7.
22. Matheron G. Principles of geostatistics. *Econ Geol*. 1963;58(8):1246-1266.
23. Bachoc F. Parametric estimation of covariance function in Gaussian-process based Kriging models. Application to Uncertainty Quantification for Computer Experiments 2013.
24. Diamond P, Armstrong M. Robustness of variograms and conditioning of kriging matrices. *Math Geol*. 1984;16(8):809-822.
25. Gratton Y. Le krigeage: la méthode optimale d'interpolation spatiale. *Les Artic l'Institut d'Analyse Géographique*. 2002;1-4.
26. Jumel J, Budzik MK, Ben Salem N, Shanahan MER. Instrumented end notched flexure—crack propagation and process zone monitoring. Part I: modelling and analysis. *Int J Solids Struct*. 2013;50(2):297-309.
27. Salem NB, Budzik MK, Jumel J, Shanahan MER, Lavelle F. Investigation of the crack front process zone in the double cantilever beam test with backface strain monitoring technique. *Eng Fract Mech*. 2013;98:272-283.
28. Badulescu C, Cognard JY, Créac'Hcadec R, Vedrine P. Analysis of the low temperature-dependent behaviour of a ductile adhesive under monotonic tensile/compression-shear loads. *Int J Adhes Adhes*. 2012;36:56-64.
29. Cognard JY, Créac'hcadec R, da Silva LFM, Teixeira FG, DAvies P, Peleau M. Experimental analysis on the influence of hydrostatic stress on the behaviour of an adhesives using a pressure vessel. *J Adhes*. 2011;87:1-16.
30. Cognard JY, Créac'hcadec R, Sohier L, Davies P. Analysis of the nonlinear behavior of adhesives in bonded assemblies-comparison of TAST and Arcan tests. *Int J Adhes Adhes*. 2008;28(8):393-404.
31. Castagnetti D, Spaggiari A, Dragoni E. Robust shape optimization of tubular butt joints for characterizing thin adhesive layers under uniform normal and shear stresses. *J Adhes Sci Technol*. 2010;24(11-12):1959-1976.
32. Moradi A, Carrère N, Leguillon D, Martin E, Cognard JY. Strength prediction of bonded assemblies using a coupled criterion under elastic assumptions: effect of material and geometrical parameters. *Int J Adhes Adhes*. 2013;47:73-82.
33. Weißgraeber P, Becker W. A coupled stress and energy model for mixed-mode cracking of adhesive joints. 13th Int Conf Fract 2013:1–8.
34. Stone M. Cross-validatory choice and assessment of statistical predictions. *J R Stat Soc*. 1974;36:111-147.